VALVELESS PRESSURE REGULATION WITH A SUBMERGED MICRO-HOLE

Ping-Hei Chen*, Jin-Cherng Shyu, and Wen-Feng Cheng
Department of Mechanical Engineering
National Taiwan University
Taipei, Taiwan 106, R.O.C.

Key Words: bubble, detached bubble volume, pressure fluctuation, correlation.

ABSTRACT

This study aims at controlling air pressure fluctuation in a chamber from which liquid is being drained continuously by using a submerged micro-hole. In practical applications, this test chamber is used to simulate the commercial ink cartridge of a thermal bubble inkjet printhead. The chamber air pressure drops owing to liquid being drained from the chamber, and it rises again as bubbles are generated and detached from a submerged micro-hole connecting liquid and the atmosphere. The chamber air pressure fluctuation can be controlled in a designated range that depends on factors such as physical properties of liquid used in the chamber, micro-hole diameter, and liquid drain rate. In this study, both distilled water and 10% wt. isopropanol solution are tested with micro-hole diameter ranging from 60 to 1200 μm. To simulate practical ink injection rates, the liquid drain rate ranges from 0.006 to 0.10 ml/s. For conditions tested in this study, our measured results show that the chamber air pressure variation and detached bubble volume depend mainly on micro-hole diameter and physical properties of liquid, and only slightly on liquid drain rate. Two correlations are proposed to obtain both the detached bubble volume and chamber air pressure fluctuation from physical properties of liquid and micro-hole diameter.

I. INTRODUCTION

In many engineering applications, systems have small openings with gas-liquid interfaces, such as the ink cartridge of a thermal bubble ink printhead or an intravenous drip. A pressure difference might occur at the interface, and it can drive bubble formation once it reaches a threshold value. If this bubble formation process takes place in a liquid filled chamber at a hole that connects liquid and the atmosphere, the criterion determining bubble generation and detachment is controlled by the force balance among surface tension force, buoyant force, inertial force and pressure difference at the interface. The detached bubbles will increase the chamber air pressure while they float through liquid, and break at the upper liquid level.

There are several factors that would affect detached bubble volume at a submerged orifice or micro-hole, such as orifice diameter, physical properties of liquid, submergence and so on. Blanchard and

*Correspondence addressee

Syzdek (1977) conducted measurements to study the effect of orifice diameter on detached bubble volume. In their study, bubbles were formed at several capillary tubes with different diameters ranging from 1.6 to 2800 μm at very low gas flow rate, to model the quasi-static bubble formation process. Under such operating conditions, the detached air bubble volumes, in water, were successfully predicted by a correlation, given by

$$V_b = \frac{\pi D_h \sigma}{(\rho_l - \rho_g)g} \tag{1}$$

However, Eq. (1) is only valid in a static bubbling regime, as mentioned by McCann and Prince (1971) for cases in which bubbling frequency is less than 0.5 Hz (Wilkinson and van Dierendock, 1994). As gas flow rate increases, the downward forces exerted on bubbles, such as the viscous force and inertial force, become significant.

However, for some practical applications, there is no gas chamber beneath a submerged hole of micro-size, such as a bubble generator in a thermal bubble inkjet printhead (Cowger, 1992) in Fig. 1(a). Since ink is required to be fed quickly into the micro-channels of the printhead from the ink cartridge, it is critical to keep the chamber air pressure in the cartridge at a designated level. Otherwise, the printing quality of a printhead can be affected by inadequate pressure supplemented by the rupture of air bubbles in the ink cartridge. Unfortunately, few measured data have been reported with experimental setup corresponding to this kind of bubble generation application.

Bubbles are generated in a bubble generator owing to an increasing pressure difference between the atmosphere and the gas space in the ink cartridge while ink is being continuously ejected in the printing process. There is no doubt that the frequency of bubble generation varies with ink ejection rates. Bubble generation frequency that increases with ink ejection rate can shift the bubbling regime from static to dynamic. However, Eq. (1) only reflects the force balance between buoyancy and surface tension, as such it might not be sufficient to predict detached bubble volume under various operating conditions.

To understand bubble formation mechanism in a system simulating an ink cartridge, Shyu *et al.* (2002a) first applied a modified spherical one-stage bubble formation model to predict detached bubble volume at a submerged micro-hole with liquid drainage in a test chamber as shown in Fig. 1(b). The hole diameters ranged from 60 to 1200 μm in their study. It was found that bubble formation at hole diameters smaller than 92 μm was static. Moreover, the liquid drain rates seemed to have no significant effect on

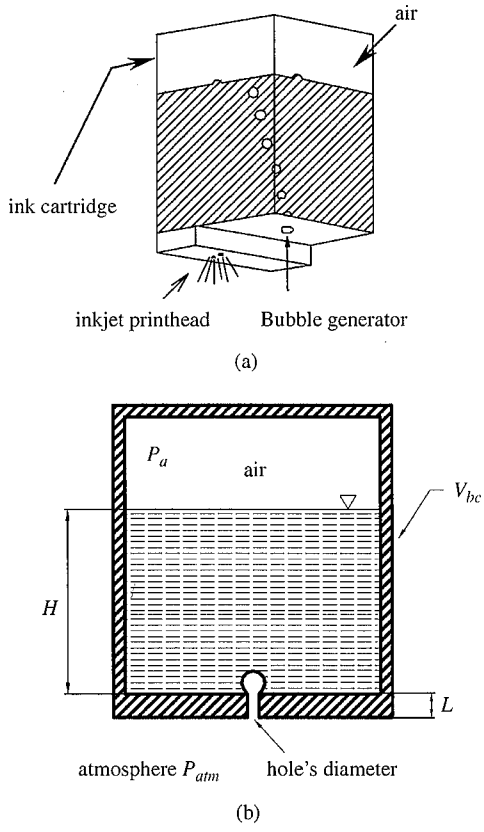

Fig. 1 (a) An inkjet printhead bubble generator; (b) Schematic diagram for dimensional analysis of bubble generation and detachment in bubble generator

detached bubble volume.

There are two aims of this study. The first one is to measure the chamber air pressure fluctuation of a liquid filled test chamber, due to liquid drainage from the chamber, and air supplement from a submerged micro-hole open to the atmosphere. The second aim is to provide correlations to obtain chamber air pressure fluctuation from hole diameter and physical properties of fluid.

II. EXPERIMENTAL METHOD

In this study, a liquid filled test chamber is used to simulate the ink cartridge of a thermal bubble printhead. A 10% wt. isopropanol solution is used to simulate the ink due to physical properties approximate to those of commercial black ink and the mixed solution is transparent. To measure the chamber air pressure and detached bubble volume, a schematic view of the experimental apparatus is shown in Fig. 2. The setup consists of four major systems, namely a liquid filled test chamber, a PC-controlled transverse system, a pressure measuring and recording system, and an image processing system. Two sidewalls of the test chamber are made of copper, and

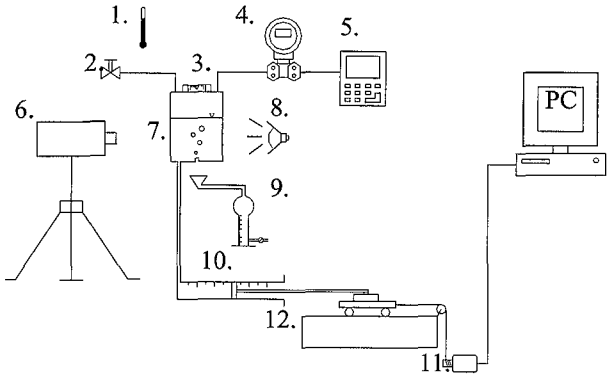

Fig. 2 Schematic view of experimental apparatus (1. Thermometer, 2. Relief valve, 3. Level gauge, 4. Differential pressure transmitter, 5. Handy recorder, 6. High-speed video camera, 7. Test chamber, 8. Halogen lamp, 9. Leakage receiver, 10. Syringe, 11. Stepping motor, 12. Platform of a linear transverse talbe)

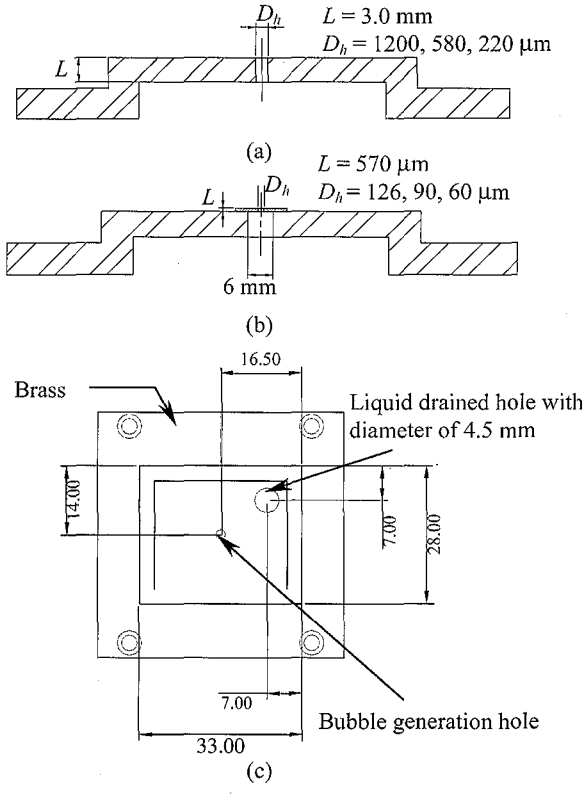

Fig. 3 Schematic views of test plate, (a) a driller-drilled hole; (b) a laser-drilled hole; (c) top view of the bottom plate, unit: mm

the other two are transparent acrylic. The bottom plate of the chamber has two holes, one for liquid drainage and the other for bubble generation. The bottom plate is replaceable with test pieces of various micro-hole diameters. For hole diameters 1200, 580 and 220 μm, the micro-hole is drilled on a brass

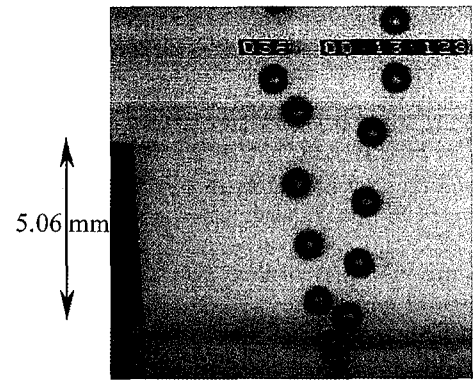

Fig. 4 Visualized result of air bubble generation in water from a test plate at D_h=60 μm and Q_d=0.1 ml/s

plate with an uncertainty of 5 μm; for diameters of 126, 90, 60 μm, the micro-hole is drilled on a polycarbonate sheet by an excimer laser (193nm, Lambda Physik) with an uncertainty within 1 μm. No gas chamber is used; the bottom end of the hole is open to the atmosphere.

A PC-controlled transverse system is used for liquid drainage at a fixed rate during measurement. The drainage hole is connected to a syringe fixed on a linear transverse table that is controlled by a stepping motor. Six preset liquid drain rates (Q_d), 0.006, 0.01, 0.02, 0.035, 0.05, and 0.10 ml/s, are respectively tested for each micro-hole, and a total amount of 10 ml will be drained for each test. During measurement, a differential pressure transmitter (FOXBORO IDP10-A) with measuring range of 20 kPa, was used to measure the unsteady pressure fluctuation between the atmosphere and the chamber air pressure, at an uncertainty of 20 Pa. The unsteady pressure signals were transmitted to a recorder (YOKOGAWA, OR141-2/L2/PM) at a sampling rate of 16 Hz.

An image processing system consists of a high-speed video camera (NAC color HSV-1000) with a capture rate of 1000 frames/sec and a shutter speed of 1/2500 second, and a high power halogen lamp used for taking high quality pictures. The recorded images were transmitted to a personal computer for image analysis and to evaluate the volume of detached bubbles. As shown in Fig. 4, images were captured synchronously with the recorded pressure during measurement. In addition, a personal computer was also used for image analysis to obtain the volume of detached bubbles, V_b, as experimental data. Although the detached bubbles are not perfect spherical shapes, but more likely ellipsoids as shown in Fig. 4, the boundaries of bubbles can still be easily found through proper image processing procedures and can be used to determine bubble volume by integration. For each measurement, the detached bubble volume

Table 1 Experimental conditions

Item	Conditions	
Liquid used	Water	10% w.t. Isopropanol sol.
Dynamic viscosity of water, μ_l	8.9×10^{-4} Pa·s	1.51×10^{-3} Pa·s
Density of water, ρ_l	1000 kg/m^3	996 kg/m^3
Surface tension of water, σ	72×10^{-3} N/m	39×10^{-3} N/m
Gas used	Air	
Dynamic viscosity of gas, μ_g	1.81×10^{-5} Pa·s	
Density of gas, ρ_g	1.205 kg/m^3	
Test conditions		
Inner dimension of test chamber	2.8×3.3×3.8 cm^3	
Initial height of liquid level	3.5 cm	
Hole diameters, D_h	1200, 580, 220, 126, 90, 60 μm	
Hole length, L	3 mm	for D_h=1200, 580 and 220 μm
	570 μm	for D_h=126, 90, and 60 μm
Liquid drain rate, Q_d	0.006, 0.01, 0.02, 0.035, 0.05, and 0.10 ml/s	
Drained volume	1.97 cm^3/rev of the stepping motor	
Total amount of drainage	10 ml	
Ambient temperature	24±1°C	

is determined by taking an average value of 10 bubbles just detached from the hole, with maximum deviation of approximately 3%. The maximum uncertainty of calculating bubble volume from the images is about 7%, depending on the measured accuracy and pixel resolution.

The experimental conditions are listed in Table 1. A leakage test was carried out before each measurement. For further details of experimental procedures, please refer to Shyu *et al.* (2002a).

III. RESULTS AND DISCUSSIONS

It was verified by Shyu *et al.* (2002a) that the liquid drain rate has no significant effect on detached bubble volume, despite the different liquid drain rates used in this study. For most operating conditions tested in this study, a typical zigzag pattern of the driving pressure difference variation, dP, versus time is shown in Fig. 5. Based on the definition of driving pressure difference given in this study, $dP=P_{atm}-P_a-\rho_l gH$, the value of dP rises with a decrease in chamber air pressure, P_a, due to liquid drainage from the test chamber. When dP reaches a threshold value, $4\sigma/D_h$ (Shyu *et al.*, 2002a), air bubbles start to form, to detach, to float through liquid, and to break at the upper air-liquid interface. Before the generated bubble reaches the upper air-liquid interface, dP continuously increases to a maximum value, dP_{max}. Since the time durations for detached bubbles to float through fluid is short, dP_{max} is slightly higher than $4\sigma/D_h$. As air bubbles break at the upper air-liquid interface, dP

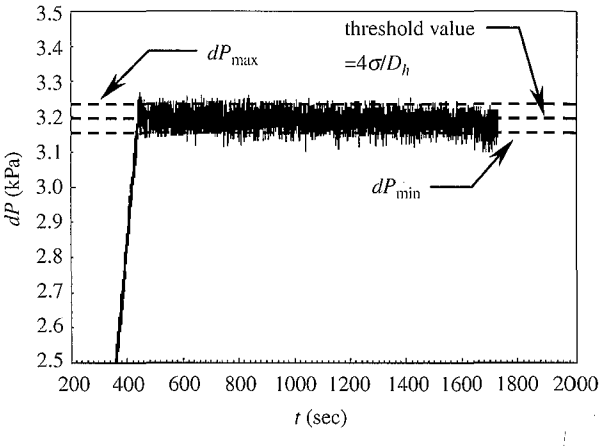

Fig. 5 Driving pressure difference with time for D_h=90 μm and Q_d=0.006 ml/s in a water chamber

immediately drops because the air supply rate from the atmosphere into the air chamber is faster than the liquid drain rate. Once dP drops to a lower limit, dP_{min}, air bubble generation stops. Then, dP is expected to rise again. The two limits of driving pressure difference, dP_{min} and dP_{min}, are illustrated as horizontal dashed lines in Fig. 5. This periodic phenomenon of stop-and-go air bubble generation results in the zigzag pattern of driving pressure difference. It is worth noting that driving pressure difference stays between these two limiting values if the hole diameter is chosen regardless of liquid drain rate. If changes in the atmospheric pressure and liquid level can be neglected during each measurement, chamber

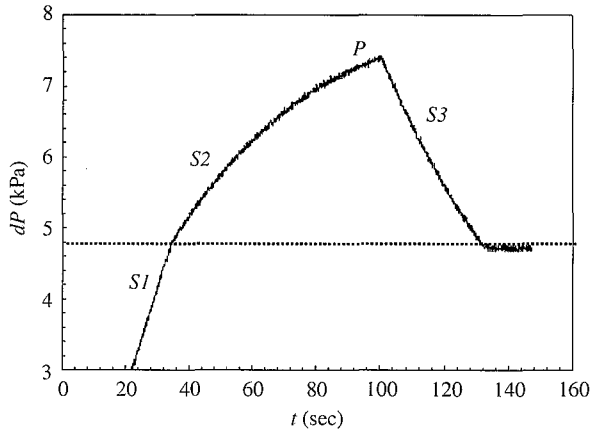

Fig. 6 Driving pressure difference with time for an unregulated case at D_h=60 μm and Q_d=0.1 ml/s in a water chamber

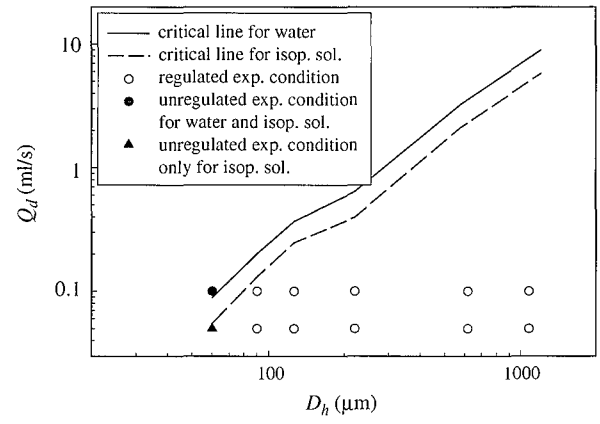

Fig. 7 Limits for regulated cases with a submerged micro-hole in this study

air pressure is kept in a specified range that lies between dP_{max} and dP_{min}. Consequently, chamber air pressure is regulated in a range between dP_{max} and dP_{min} of which the values depend on the diameter of submerged micro-hole and physical properties of fluid.

For the operating conditions tested, most of the measurements of driving pressure difference variation are similar to the one shown in Fig. 5. However, there is one unregulated case, as shown in Fig. 6. Figure 6 shows that the driving pressure difference for bubble generation in water at D_h= 60 μm, the smallest hole tested, and Q_d=0.1 ml/s, the highest drain rate tested. This driving pressure difference response has two positive slopes, $S1$, $S2$; and one negative slope, $S3$. It is expected that the driving pressure difference rises sharply at the beginning of liquid drainage because no air supplement from bubble generation can be observed before the driving pressure difference reaches a threshold value. Thus, a sharp slope, $S1$, can be found in the driving pressure difference response at the initial stage of liquid drainage. When the driving pressure difference reaches the threshold value for bubble generation as shown in the dashed line in Fig. 6, air bubbles begin to form and to detach. However, the detached bubble volume is so small, as shown in Fig. 4, that the air supplement rate into air chamber is far less than the pressure drop rate from liquid drainage. The driving pressure difference thus continues to increase with a flatter slope, $S2$, than $S1$. The drainage stops when a designated amount, 10 ml of liquid, is drained out of the test chamber. It is thus expected that the driving pressure difference reaches its peak value at the time when drainage stops, and then drops with a negative slope of $S3$ because bubbles continue to generate. The driving pressure difference continues to drop until it reaches a value close to but less than the threshold value. Then, the driving pressure difference should remain flat. However, some fluctuations can still be observed and it is believed to be pressure sensor noise. The same phenomena can be found in 10%wt isopropanol solution at D_h= 60 μm and Q_d=0.1 ml/s, but not in any other tested cases. For the driving pressure difference shown in Fig. 6, the chamber air pressure fluctuation cannot be controlled in a designated range between two limit values, dP_{max} and dP_{min}.

In this study, it becomes important to identify the tested conditions under which chamber air pressure cannot be regulated under a fixed drain rate with a submerged micro-hole. As expected, these unregulated cases will occur when the liquid drainage rate is faster than the air supplement rate, $Q_d > V_b \times F$ where F is bubble generation frequency. The definition of bubble generation frequency is well known as proposed by Zhang and Tan (2000), $F=1/(t_{weeping}+t_w+t_{bf})$ where $t_{weeping}$ is the weeping time, t_w is the waiting time and t_{bf} is the bubble formation time. However, both $t_{weeping}$ and t_w are considerably smaller than t_{bf}. Therefore, a tested case is unregulated with a liquid drain rate above a critical value that is approximately defined as $V_b/t_{bf}=Q_{d,crit}$. Furthermore, a modified two-stage bubble formation model that is proposed by Shyu *et al.* (2002) can be used to calculate both values of tbf and V_b.

The predicted critical liquid drain rates versus hole diameter are shown in Fig. 7 for both liquids tested in this study. It can be observed that any tested condition lying below the solid and dashed lines is a regulated case. This finding is confirmed by the measured results, shown as hollow circles in Fig. 7. In addition, a triangular symbol representing Q_d=0.05 ml/s and D_h=60 μm is located to the right of the dashed line, but below the solid line. One can conclude that the test condition with Q_d=0.05 ml/s and D_h=60 μm is regulated for water but becomes

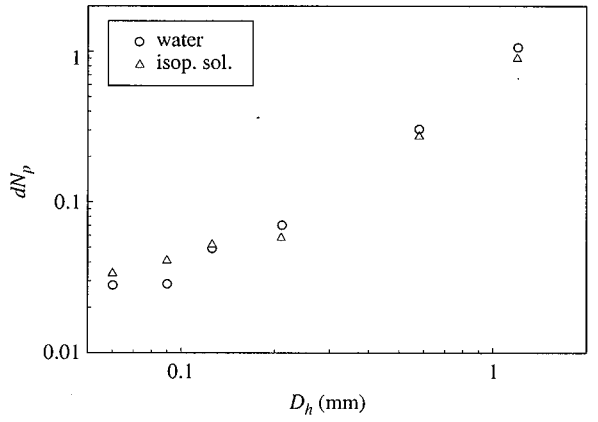

Fig. 8 Variation of N_p with hole diameters at Q_d=0.006 ml/s for water and 10% w.t. isopropanol solution

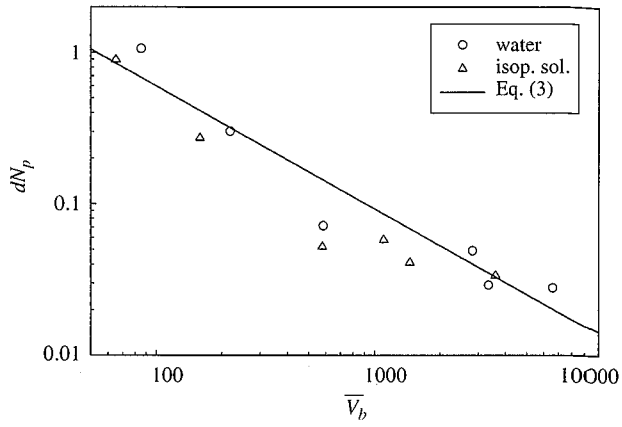

Fig. 9 A correlation for dN_p versus $\overline{V}_b$

unregulated for 10% wt isopropanol. Our measured data confirm this observation, too. To assure printing quality, it becomes more important for designers to ensure the cartridge air pressure being regulated with a designated diameter of micro-hole because higher dpi and ink ejection frequency are used in better inkjet printheads.

For practical applications, empirical correlations should be provided from our measured results to obtain driving pressure difference from hole diameter and physical properties of fluid in a chamber. To reduce the number of variables in the correlations, a dimensional analysis is performed to obtain a relation that dimensionless driving pressure difference depends on several important dimensionless groups, expressed as

$$\frac{dP}{4\sigma/D_h} = f\left(\frac{V_b}{D_h^3}, \frac{\Delta\rho g D_h^2}{\sigma}, \frac{L}{D_h}, \frac{\mu_l}{\sqrt{D_h\sigma\Delta\rho}}\right) \qquad (2a)$$

and

$$N_p = f\left(\overline{V}_b, Bo, \frac{L}{D_h}, \frac{\mu_l}{\sqrt{D_h\sigma\Delta\rho}}\right) \qquad (2b)$$

where $N_p = \frac{dP}{4\sigma/D_h}$ denotes dimensionless driving pressure difference, $\overline{V}_b = \frac{V_b}{D_h^3}$ denotes dimensionless detached bubble volume, $Bo = \frac{\Delta\rho g D_h^2}{\sigma}$ denotes Bond number, and $\Delta\rho$ denotes the density difference between liquid and air.

For the operating conditions tested in this study, the value of N_p is slightly affected by the third and fourth dimensionless groups listed on the right hand side of Eq. (2b). Davidson and Schuler (1960) recommended that the effect of viscosity of water on bubble formation is insignificant. Thus, the effect of dimensionless group, $\frac{\mu_l}{\sqrt{D_h\sigma\Delta\rho}}$, on dimensionless driving pressure difference is ignored in the present study because the values of $\frac{\mu_l}{\sqrt{D_h\sigma\Delta\rho}}$ of both liquids are less than 10^{-2}.

Although L/D_h could be important to detached bubble volume (Kumar and Kuloor, 1970), the effect of L/D_h over the range in the present study on dimensionless driving pressure difference is believed to be insignificant. The bubble formation mechanism among all hole diameters tested in this study can be approximated as the case at constant flow condition (Shyu *et al.*, 2002b).

It should be stated again that the regulated range of driving pressure difference in Fig. 7 can be assumed to be approximately the same as regulated range of chamber air pressure if the changes in the atmosphere and hydrostatic pressure of liquid are neglected. Thus, the regulated range of chamber air pressure is obtained once the regulated range of driving pressure difference can be calculated from correlations proposed in this study. The dimensionless fluctuation of driving pressure difference is defined as, dN_p=$N_{p,\max}$–$N_{p,\min}$ where $N_{p,\max}$ and $N_{p,\min}$ respectively correspond to the maximum and the minimum driving pressure difference, $dP_{\max}$ and $dP_{\min}$ in Fig. 5. The variations of dN_p with hole diameter for both water and 10% w.t. isopropanol are shown in Fig. 8. It is found that the fluctuation range of dimensionless driving pressure difference, dN_p, increases with hole diameter. This phenomenon is expected to occur as fluctuation of chamber air pressure is affected by the amount of air supplement into air chamber. Air supplement is directly related to detached bubble volume. The larger the hole diameter is, the larger detached bubble volume is obtained.

The variation of dN_p with $\overline{V}_b$ is plotted in Fig. 9 from our measured data. The best fit to the data is given by

$$dN_p = 25\overline{V}_b^{-0.81} \qquad (3)$$

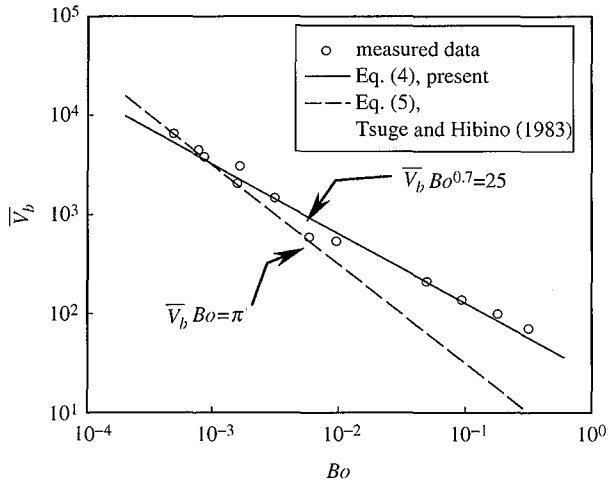

Fig. 10 A comparison with a previous correlation by Tsuge and Hibino (1983) for $\overline{V}_b$ versus Bo

It is surprising to find that dN_p decreases with an increase in $\overline{V}_b$. However, it is due to the fact that the dimensionless bubble detached volume is defined as a ratio of the detached bubble volume to the cubic power of the hole diameter, V_b/D_h^3. Our measured results show that the increase in detached bubble diameter is slower than the increase in hole diameter. Therefore, dN_p decreases with an increase in $\overline{V}_b$.

Unfortunately, the value of $\overline{V}_b$ cannot be measured easily without an expensive image capturing system that is similar to the one shown in Fig. 2. Thus, it is reasonable to provide an empirical correlation for obtaining dimensionless bubble detached volume from hole diameter and physical properties of fluid.

In Fig. 10, the measured dimensionless detached bubble volume is plotted against Bond number. The best fit to the data is given by Eq. (4)

$$\overline{V}_b Bo^{0.7} = 25.0 \text{ at } \frac{\mu_l}{\sqrt{D_h \sigma \Delta\rho}} < 10^{-2} \tag{4}$$

Note that Eq. (4) is only valid to predict bubble detached volume for $N_p \geq 1$, $D_h \leq 1200$ μm, $\frac{\mu_l}{\sqrt{D_h \sigma \Delta\rho}} < 10^{-2}$, and $Q_d \leq Q_{d,crit}$ at a submerged micro-hole. An additional correlation shown in Fig. 10 was recommended by Tsuge and Hibino (1983) and was expressed as

$$\overline{V}_b Bo = \pi \tag{5}$$

This correlation provided by Tsuge and Hibino (1983) is for bubble formation under constant flow condition. Eq. (5) has the same form of $\overline{V}_b = f(Bo)$ as the one obtained from the present study. However, the variation in gas flow rate was not included in their study, either. The reason is that the gas flow rate used in their study was quite small. From the visualized results by Cheng (2001), bubble coalescence was observed for hole diameter greater than 126 μm for valveless pressure regulation with a submerged micro-hole. This bubble coalescence phenomenon indicates that the effect of gas flow rate on detached bubble volume cannot be neglected (Miyahara *et al.*, 1983). Since the gas flow rate has an effect on detached bubble volume at larger micro-holes, our correlation deviates from Eq. (5) at larger Bond numbers.

Combining both Eqs. (3) and (4), it yields

$$dN_p = 1.843 Bo^{0.567} \tag{6}$$

in which the fluctuation of driving pressure difference can be predicted directly from the hole diameter and physical properties of fluid.

IV. CONCLUSIONS

For a chamber partially filled with liquid with a constant or variable liquid drain rate, such as the ink cartridge of an inkjet printhead, the fluctuation range of chamber air pressure can be controlled by a submerged micro-hole. This regulation mechanism has advantages of simplicity, no moving part for fatigue failure, and low cost. An empirical correlation is proposed to predict the dimensionless driving pressure difference fluctuation from the hole diameter and physical properties of fluid in the test chamber, given by $dN_p = 1.843 Bo^{0.567}$ for $D_h \leq 1200$ μm, $\frac{\mu_l}{\sqrt{D_h \sigma \Delta\rho}} < 10^{-2}$, and $Q_d < Q_{d,crit}$ at a submerged micro-hole. Note that $Q_{d,crit}$ must be recalculated by the model given by Shyu *et al.* (2002) if the fluid used is not distilled water or 10% w.t. isopanpanol. The fluctuation range of chamber air pressure can be obtained from the fluctuation range of dimensionless driving pressure difference, dN_p. Further studies should be conducted to extend this empirical correlation to a wider range than the present tested conditions at a non-spherical hole.

ACKNOWLEDGEMENT

The authors greatly appreciate the financial support by the National Science Council R.O.C. (NSC 89-2212-E-002-117).

NOMENCLATURE

Bo	Bond number
D_h	diameter of bubble formation hole, [m]
dP	driving pressure difference, [Pa]
H	liquid height in the test chamber, [m]

L hole length, [m]
N_p dimensionless driving pressure difference,
Q_d liquid drain rate, [ml/s]
$Q_{d,crit}$ critical liquid drain rate, [ml/s]
V_b detached bubble volume, [m^3]

Greek Symbols

σ surface tension, [N/m]
ρ density, [kg/m^3]
μ viscosity, [Pa · s]

Subscripts

g gas
l liquid
max maximum value
min minimum value

REFERENCES

1. Blanchard, D. C., and Syzdek, L. D., 1977, "Production of Air Bubbles of a Specified Size," *Chemical Engineering Science*, Vol. 32, pp. 1109-1112.
2. Cheng, W. F., 2001, "Visualization of Bubble formation and Measurement of Pressure at a Single Submerged Micro-Hole," *Master Thesis*, National Taiwan University, Taipei, Taiwan, ROC.
3. Cowger, B., 1992, "The Optimization of Deliverable Ink from a Disposable Print Cartridge," *IGST's Eighth International Congress on Advances in Non-Impact Printing Technologies*, Society of IS&T, Virginia, pp. 312-317.
4. Davidson, J. F., and Schuler, B. O. G., 1960, "Bubble Formation at an Oorifice in an Inviscid Liquid," *Transactions of the Institution of Chemical Engineers*, Vol. 38, pp. 335-342.
5. Hayes, W. B., Hardy, B. W., and Holland, C. D., 1959, "Formation of Gas Bubbles at Submerged Orifices," *AIChE Journal*, Vol. 5, pp. 319-324.
6. Hughes, R. R., Handlos, A. E., Evans, H. D., and Maycock, R. L., 1955, "The Formation of Bubbles at Simple Orifices," *Chemical Engineering Progress*, Vol. 51, pp. 557-563.
7. Iliadis, P., Douptsoglou, V., and Stamatoudis, M., 2000, "Effect of Orifice Submergence on Bubble Formation," *Chemical Engineering Technology*, Vol. 23, pp. 341-345.
8. Kumar, R., and Kuloor, N. R., 1970, "The Formation of Bubbles and Drops," *Advances in Chemical Engineering*, Academic Press, New York, USA.
9. McCann, D. J., and Prince, R. G. H., 1971, "Regimes of Bubbling at a Submerged Orifice," *Chemical Engineering Science*, Vol. 26, pp. 1505-1512.
10. Miyahara, T., Haga, N., and Takahashi, T., 1983, "Bubble Formation from an Orifice at High Gas Flow Rates," *International Chemical Engineering*, Vol. 23, pp. 524-531.
11. Shyu, J. C., Ding, P. P., Cheng, W. F., and Chen, P. H., 2002a, "Air Bubble Generation Through a Submerged Micro-Hole," *Chemical Engineering Research & Design*, Vol. 80, pp. 355-363.
12. Shyu, J. C., Ding, P. P., and Chen, P. H., 2002b, "Study on Bubble Formation at a Submerged Micro-Hole by a Two-Stage Model," Private Communication.
13. Takahashi, T., and Miyahara, T., 1976, "Bubble Volume Formed at Submerged Nozzles: Constant Gas Flow Condition," *Kagaku Kogaku Ronbunshu*, Vol. 2, pp. 138-143.
14. Tsuge, H., and Hibino, S. I., 1978, "Bubble Formation from a Submerged Single Orifice Accompanied by Pressure Fluctuations in Gas Chamber," *Journal of Chemical Engineering of Japan*, Vol. 11, pp. 173-178.
15. Wilkinson, P. M., and van Dierendock, L. L., 1994, "A Theoretical Model for the Influence of Gas Properties and Pressure on Single Bubble Formation at an Orifice," *Chemical Engineering Science*, Vol. 49, pp. 1429-1438.
16. Zhang, W., and Tan, R. B. H., 2000, "A Model for Bubble Formation and Weeping at a Submerged Orifice," *Chemical Engineering Science*, Vol. 55, pp. 6243-6250.

Manuscript Received: Oct. 04, 2001
Revision Received: Mar. 07, 2002
and Accepted: Apr. 01, 2002

以單微孔進行無閥的壓力調控

陳炳煇　徐金城　鄭文峰

國立台灣大學機械工程系

摘　要

本研究旨在以一液面下的單微孔產生氣泡，以控制容器內因液體逐漸排出而造成容器內空氣壓力的下降，因容器內壓力降到一定程度，將使容器底部因與大氣連接之微孔口產生氣泡，而使容器內的空氣壓力因氣泡浮到液面破裂而獲得補充而上升。實際上，此種機制已被使用在商用的熱氣泡式噴墨印表頭的墨水匣中的壓力調控。亦即此種裝置可藉由容器內液體的性質，微孔口的尺寸及液體排出速度以控制容器內的壓力震盪在一定的範圍內。本實驗使用兩種流體進行測試，分別爲純水及重量百分比濃度10%的異丙醇水溶液，測試的微孔口直徑介於 60 到 1200 μm ，液體的排出速度介於 0.006 到 0.1 ml/s 。吾人的實驗結果顯示，容器內的壓力震盪主要與容器內的液體性質及微孔口尺寸有關，與液體的排出速度關聯較不明顯。此研究亦提出了兩關聯式，分別計算容器內壓力震盪與氣泡脫離體積與流體性質及微孔口尺寸的關係。

關鍵詞：氣泡，氣泡脫離體積，壓力震盪，關聯式。